Purification and Physical-Chemical Characterization of the Three Hydroperoxidases from the Symbiotic Bacterium *Sinorhizobium meliloti*†

Silvia Ardissone,‡ Pierre Frendo,§ Enzo Laurenti,‡ Walter Jantschko,|| Christian Obinger,|| Alain Puppo,§ and Rosa Pia Ferrari*,‡

Dipartimento di Chimica I. F. M., Università di Torino, via Pietro Giuria 7, 10125 Torino, Italy, UMR CNRS-INRA-Université de Nice-Sophia Antipolis IPMSV 400, Route des Chappes, BP167, 06903 Sophia-Antipolis Cedex, France, and Department of Chemistry, Division of Biochemistry, BOKU, University of Natural Resources and Applied Life Sciences, A-1180 Wien, Austria

Received June 7, 2004; Revised Manuscript Received July 13, 2004

ABSTRACT: Three genes encoding heme hydroperoxidases (*katA*, *katB*, and *katC*) have been identified in the soil bacterium *Sinorhizobium meliloti*. The recombinant proteins were overexpressed in *Escherichia coli* and purified in order to achieve a spectral and kinetic characterization. The three proteins contain heme *b* with high-spin Fe(III). KatB is an acidic bifunctional homodimeric catalase-peroxidase exhibiting both catalase ($k_{cat} = 2400\ s^{-1}$) and peroxidase activity and having a high affinity for hydrogen peroxide (apparent $K_M = 1.6$ mM). KatA and KatC are acidic monofunctional homotetrameric catalases. Although different in size (KatA is a small subunit catalase while KatC is a large subunit catalase) both enzymes exhibit the same heme type and a similar affinity for H_2O_2 (apparent K_M values of 160 and 150 mM). However, the turnover rate of KatA ($k_{cat} = 279000\ s^{-1}$) exceeds that of KatC ($k_{cat} = 3100\ s^{-1}$) significantly. The kinetic parameters are in good agreement with the physiological role of these heme proteins. KatB is the housekeeping hydroperoxidase exhibiting the highest affinity for hydrogen peroxide, while KatA has the lowest H_2O_2 affinity but the highest k_{cat}/K_M value ($1.75 \times 10^6\ M^{-1}\ s^{-1}$), in agreement with the hydrogen peroxide inducibility of the encoding gene. Moreover, the lower catalytic efficiency of KatC ($2.1 \times 10^4\ M^{-1}\ s^{-1}$) appears to be enough for growing in the stationary phase and/or under heat or salt stress (conditions that are known to favor *katC* expression).

Cellular metabolism of dioxygen (O_2) is essential to aerobic organisms but can lead to the production of reactive cytotoxic species such as singlet oxygen, superoxide ($O_2^{\bullet -}$), hydrogen peroxide (H_2O_2), and hydroxyl ($OH^{\bullet}$) radical, which can damage cellular components by oxidizing lipids, proteins, and nucleic acids (*1*). To avoid these effects, cells growing under aerobic conditions possess specific enzymatic systems to maintain reactive oxygen species (ROS) at nonharmful levels (*2*). Hydroperoxidases are oxidoreductases involved in hydrogen peroxide degradation. Among others, they include heme-containing monofunctional catalases and peroxidases, which are ubiquitous enzymes (*3*−*5*).

Monofunctional catalases (EC 1.11.1.6) show a remarkable level of conservation in both their core sequences and structural features. One group contains small subunit enzymes (55−69 kDa) with heme *b* associated and one contains large subunit enzymes (75−84 kDa) with heme *d* associated (*3*). Regarding their predominant activity, i.e., the dismutation of hydrogen peroxide to water and molecular oxygen, striking variations are found in specific activities, reaction velocities, and sensitivity to high concentrations of hydrogen peroxide (*3*, *6*, *7*).

Peroxidases (EC 1.11.1.7) are more heterogeneous and categorized in two superfamilies: one heme *b* containing superfamily including enzymes from bacteria, fungi, and plants (*4*) and one superfamily containing animal peroxidases containing a modified heme *b* (*5*). Peroxidases use hydrogen peroxide to oxidize a great variety of both inorganic and organic substrates (i.e., the *peroxidatic* activity). Catalase-peroxidases, being homologous with plant ascorbate peroxidases and fungal cytochrome *c* peroxidases (*8*), are the only peroxidases which can oxidize hydrogen peroxide by releasing molecular oxygen (i.e., the *catalatic* activity) at reasonable rates with k_{cat}/K_M values comparable with those of monofunctional catalases. Indeed, catalase-peroxidases are bifunctional, having also in addition a peroxidase activity of broad specificity (*9*, *10*). Bacterial catalase-peroxidases (hydroperoxidases I) have been isolated from a variety of different organisms of both prokaryotic and lower eukaryotic origin (*9*−*13*).

Regarding the physiology of catalase expression and its control in bacteria, *Escherichia coli* is well studied. *E. coli* contains two *catalatically* active enzymes, namely, HPI[1] and HPII. The catalase-peroxidase (HPI) is mainly expressed upon induction of oxidative stress, whereas the levels of the

† This work was supported by the Italian MIUR (Ministero per l'Istruzione, l'Università e la Ricerca).

* To whom correspondence should be addressed. Tel: +39 011 670 7516. Fax: +39 011 670 7855. E-mail: rosapia.ferrari@unito.it.

‡ Università di Torino.

§ UMR CNRS−INRA-Université de Nice.

|| University of Natural Resources and Applied Life Sciences.

[1] Abbreviations: HPI, hydroperoxidase I; HPII, hydroperoxidase II; KatB, catalase−peroxidase; KatA and KatC, monofunctional catalases; DMAB, 3-(dimethylamino)benzoic acid; MBTH, 3-methyl-2-benzothiazolinone hydrazone hydrochloride; ABTS, 2,2′-azinobis(3-ethylbenzothiazoline-6-sulfonic acid); IPTG, β-D-thiogalactopyranoside.

10.1021/bi048836s CCC: $27.50
Published on Web 09/09/2004

monofunctional catalase (HPII) increase as cells grow into stationary phase. The role of HPII seems to be protection during periods of slow or no growth (*14*, *15*).

Interestingly, in the completely sequenced genome of the Gram-negative soil bacterium *Sinorhizobium meliloti*, three genes encoding heme-containing and *catalatically* active hydroperoxidases can be found, belonging to the three distinct groups mentioned above: *katA*, encoding a monofunctional catalase with heme *b*, *katC*, encoding a large subunit monofunctional catalase, and, finally, *katB*, encoding a catalase-peroxidase (*16*−*19*). *S. meliloti* is able to develop a symbiosis with some *Medicago* species (*Medicago sativa* and *Medicago truncatula*), and this plant-bacterium interaction leads to the formation of root nodules (*20*); during this process, bacteria differentiate to their symbiotic forms, the so-called bacteroids, which are able to reduce atmospheric nitrogen to ammonia. The expression of the three genes, *katA*, *katB*, and *katC*, is differentially regulated both during the development of the nodule and in the different phases of growth of the free-living cells (*21*, *22*). In the free-living cells, only the expression of *katA* is increased by the exposure to H_2O_2, while the induction of *katC* depends on heat stress, salt stress, and ethanol, and *katB* is not induced by any of the tested treatments (*21*, *22*). The hydroperoxidases of *S. meliloti* appear to play an important role in the symbiotic process, since *katA*$^-$−*katC*$^-$ and *katB*$^-$−*katC*$^-$ double mutants show a significant decrease in their ability to form nodules (the differentiation of bacteroids is blocked at different steps) and to fix nitrogen (*21*, *22*).

Why does *S. meliloti* utilize three different heme-containing enzymes with catalase activity? To correlate the physiological role(s) of these enzymes with defined biochemical and biophysical properties, a comparative analysis is needed. In this paper, we present the cloning, the overexpression in *E. coli*, and the purification of KatA, KatB, and KatC together with a comprehensive spectral and kinetic characterization of the enzymes. The correlation between the functional characteristics of each enzyme and its expression pattern and putative physiological role(s) is discussed.

EXPERIMENTAL PROCEDURES

Construction of the Expression Vectors. S. meliloti (strain RCR2011) was grown at 30 °C in LB medium containing 2.5 mM $MgSO_4$ and 2.5 mM $CaCl_2$ (*19*), and total DNA was prepared according to Ausubel et al. (*23*). Synthetic oligonucleotide primers were from MWG-Biotech (Germany).

The *katB* gene was amplified by using primer B1 (AAGAAGACTTCATGGATCAGAAGAGCGATAGTGC), containing a *Bbs*I restriction site and the ATG, and primer B2 (AAACTCGAGTCAGACCAGATCAAAGCGGTCG), containing the stop codon and an *Xho*I restriction site. As for the monofunctional catalases, primers A1 (AAAGGTCTCTACATGACAGATCGTCCGACGATCACC) and A2 (AAACTCGAGTTACTCGGCCGCCGTGCTGATC) were employed to amplify the *katA* gene, and primers C1 (AAACCATGGCCAAGAAACCCTCTGCGC) and C2 (AAACTCGAGCTATTTCAGCTTGACCGAGGGTTC) were used in the case of *katC*; the oligonucleotide A1 contained a *Bsa*I restriction site and the oligonucleotide C1 an *Nco*I restriction site, whereas both oligonucleotides A2 and C2 contained an *Xho*I restriction site.

All amplification reactions were composed of 35 cycles, carried out under the following conditions: denaturation, 95 °C for 30 s; annealing, 68 °C for 30 s; extension, 72 °C for 2 min; the final step of extension was prolonged to 15 min. The PCR products were fractionated on a 1% agarose gel, and the appropriate DNA was cut out, purified using the QiaEx II gel extraction kit (Qiagen), and ligated into a pGEM-T vector.

Each insert was then sequenced (MWG-Biotech) in order to verify the amplified sequence. The pGEM-T vectors containing the cloned genes were digested with the appropriate restriction enzymes, and the fragments obtained were purified and cloned into the expression vector pET-30a, digested with *Nco*I and *Xho*I.

Overexpression and Purification. Competent *E. coli* BL21-(DE3)pLysS cells were transformed with the expression vector pET-30a containing *katA*, *katB*, or *katC*; positive clones carrying the recombinant plasmid were selected and grown overnight at 37 °C with shaking in LB medium containing 30 μg/mL kanamycin and 34 μg/mL chloramphenicol. The cell suspension was diluted to get an initial OD_{600} of 0.05, and the culture was grown at 37 °C until an OD_{600} of 0.6−0.7 was obtained; the expression of the recombinant protein was then induced by the addition of 1 mM β-D-thiogalactopyranoside (IPTG); at the same time hemin was added to a final concentration of 40 μg/mL. Cells carrying pET-30*katA* or pET-30*katB* plasmid were further incubated for 3 h at 37 °C, while the *katC* culture was cooled at 20 °C after induction and incubated overnight. Cells were then harvested by centrifugation (4000*g*, 20 min, 4 °C), resuspended in lysis buffer (50 mM NaH_2PO_4, 300 mM NaCl, 10 mM imidazole, pH 8.0), incubated on ice for 30 min with 1 mg/mL lysozyme, and broken by sonication (6 × 30 s).

RNase A and DNase I were added to the solution, and after 15 min in ice the suspension was centrifuged (10000*g*, 30 min, 4 °C) to remove the cellular debris. One milliliter of nickel-charged resin (Ni-NTA Agarose, Qiagen) was added to 4 mL of the cleared lysate and mixed gently by shaking at 4 °C for 1 h; then the mixture was loaded in the column and washed twice with 4 mL of washing buffer (50 mM NaH_2PO_4, 300 mM NaCl, 20 mM imidazole, pH 8.0). Bound proteins were eluted with 2 mL of elution buffer (50 mM NaH_2PO_4, 300 mM NaCl, 250 mM imidazole, pH 8.0), and the eluted fractions were assayed for catalase activity and assessed for purity using SDS−PAGE. Active fractions were pooled and loaded on a PD-10 desalting column (Amersham Biosciences) in order to exchange the elution buffer with 10 mM phosphate buffer, pH 7.0. Protein concentrations at each purification step were determined by using the Bio-Rad protein assay kit (bovine serum albumin as standard), according to Bradford (*24*). Typically, a 200 mL culture of *E. coli* gave approximately 5 mg of each active enzyme. All of the proteins were kept at −80 °C, and their enzymatic activity remained stable for months.

Polyacrylamide Gel Electrophoresis and Gel Filtration. SDS−PAGE was carried out on 10% slab gels as described by Laemmli (*25*) using low-range prestained molecular weight standards (Bio-Rad) and the Mini-cuve Bio-Rad. Proteins on the gel were stained with Coomassie Blue. Native PAGE was performed on 7% slab gels using the Mini-cuve Bio-Rad. Catalase activity was visualized via inhibition of

diaminobenzidine oxidation by H_2O_2 in the presence of horseradish peroxidase (*26*). Isoelectric focusing (IEF) was performed on 5% slab gels with the Mini 111 IEF cell (Bio-Rad), Bio-Rad Bio-Lyte 3/10 and 3/6 ampholytes, and Sigma IEF-Mix 3.6−6.6. Protein was detected by Coomassie staining.

Gel filtration on a Superdex 200 column (1 × 20 cm) (Pharmacia) was used to determine the molecular mass of the native enzymes. The column was equilibrated with 50 mM phosphate buffer, pH 7.0, containing 0.15 M KCl and calibrated with albumin, aldolase, catalase, ferritin, and thyroglobulin (Amersham Biosciences) in the range 67−669 kDa.

Spectroscopic Measurements. The UV−visible spectra of the samples were recorded on a Unicam UV300 (Thermospectronic) double-beam spectrophotometer equipped with a magnetic stirring device and a single cell Peltier for temperature control. The molar extinction coefficient of the Soret band, the heme type, and content were determined for each protein by recording the spectral properties of the reduced heme−pyridine complex according to Furhop and Smith (*27*). To calculate the heme-to-protein stoichiometry, the concentration of the monomer was estimated by using the following extinction coefficients, $\epsilon_{276} = 78000\ M^{-1}\ cm^{-1}$ (KatA), $\epsilon_{280} = 147500\ M^{-1}\ cm^{-1}$ (KatB), and $\epsilon_{280} = 64000\ M^{-1}\ cm^{-1}$ (KatC), estimated on the basis of the amino acid compositions (protein parameter tool from ExPASy, proteomics server of the Swiss Institute of Bioinformatics, http://www.expasy.org/). Enzyme reduction was achieved by adding sodium dithionite (up to a final concentration of 120 mM) under anaerobic conditions, and the ferric-to-ferrous form transition was investigated by recording UV−visible electronic absorption within the next hour.

EPR studies were carried out on a Bruker ESP300 X-band spectrometer equipped with an Oxford Instruments ESR900A continuous flow cooling system (3.8−300 K). Enzyme adducts with cyanide for EPR and UV−visible measurements were prepared by adding KCN (final concentration 0.2 M) to a protein solution in 10 mM phosphate buffer, pH 7.0.

Catalase and Peroxidase Assays. To allow comparison of the kinetic data of KatA and KatC from *S. meliloti* with those of other monofunctional catalases, the recently published method of Switala and Loewen was applied (*7*). Catalase activity (hydrogen peroxide degradation) was measured polarographically using a Clark-type electrode (YSI 5331 Oxygen Probe) inserted in a stirred water bath at 30 °C (*28*). One unit of catalase is defined as the amount that catalyzes the formation of 1 μmol of O_2 in 1 min in a 60 mM H_2O_2 solution at pH 7.0 and 30 °C. Initial oxygen evolution was used to determine the turnover rates to minimize the inactivation caused by high peroxide concentrations. In the case of catalase-peroxidases, which are known to have lower K_M values and being even more sensitive to peroxide concentrations higher than 20 mM (*12*), a H_2O_2 concentration of 5 mM was used for determination of kinetic parameters. The pH dependence of catalase activity was measured using 50 mM buffers (citrate-phosphate, pH 4−7.5; Tris-HCl, 7.5−9; glycine-NaOH, 9−11), containing either 60 mM H_2O_2 (KatA and KatC) or 5 mM H_2O_2 (KatB). Peroxidase activity was monitored spectrophotometrically at 25 °C in 50 mM phosphate buffer, pH 7.0, using 1 mM H_2O_2 and 2 mM 3-(dimethylamino)benzoic acid (DMAB) and 40 μM 3-methyl-2-benzothiazolinone hydrazone hydrochloride (MBTH) by following the oxidation rate at 590 nm ($\epsilon_{590} = 47600\ M^{-1}\ cm^{-1}$) (*29*) or 1 mM 2,2′-azinobis(3-ethylbenzothiazoline-6-sulfonic acid) (ABTS, $\epsilon_{414} = 31100\ M^{-1}\ cm^{-1}$) (*30*). The same buffers as in the catalase measurements were used for the determination of the pH dependence of the peroxidase activity of KatB.

Stopped-Flow Spectroscopy. The stopped-flow apparatus (model SX-18MV) and the associated computer system were from Applied Photophysics (U.K.). For a total of 100 μL/shot into a flow cell with 1 cm light path, the fastest time for mixing two solutions and recording the first data point was approximately 1.5 ms. To define the actual binding rates of the ligand cyanide to native enzyme, protein samples (1−2 μM heme) were mixed with varying concentrations of cyanide in the conventional stopped-flow mode (50 mM phosphate buffer, pH 7.0). The reaction was followed at wavelengths of 425 nm (KatA), 406 nm (KatB), and 427 nm (KatC). To ensure first-order kinetics, cyanide concentrations were at least 10 times that of the enzyme. At least three determinations (2000 data points) of k_{obs} were performed for each ligand concentration, and the mean value was used in the calculation of the second-order rate constants, which were calculated from the slope of the line defined by a plot of k_{obs} versus ligand concentration.

RESULTS

Expression and Purification of Recombinant Hydroperoxidases. On the basis of the known nucleotidic sequences of *katA*, *katB*, and *katC* from *S. meliloti* (*16*−*18*), specific primers were constructed to amplify the open reading frames by PCR. The PCR fragments were verified by sequencing and cloned into the expression vector pET-30a. *E. coli* cells were then transformed with the obtained plasmids. The IPTG-induced expression of *katA*, *katB*, and *katC* was analyzed by SDS−PAGE of cell lysates (data not shown). In both total and soluble extracts obtained from cells growing at 37 °C for 3 h after induction a new protein band appeared, at 60 kDa (KatA) and 85 kDa (KatB). In the case of KatC, the overexpressed protein was totally located in inclusion bodies (data not shown). Therefore, to obtain a soluble form of KatC, the culture was grown overnight at 20 °C after induction to slow the metabolism according to Kerschbaumer et al. (*31*). This temperature change allowed to find the KatC band in the soluble fraction at an apparent molecular mass of about 85 kDa on SDS−PAGE (data not shown).

After purification (see Experimental Procedures) protein purity was estimated to be over 95% (data not shown). As a control, cellular lysates from transformed cells carrying the expression vector lacking the insert were loaded onto the affinity column. After washing, no catalase activity was detected in the eluted fractions. Recombinant proteins exhibited a substantial catalase activity when separated on nondenaturing PAGE and stained for catalase activity (data not shown).

Physical Characterization of Recombinant KatA, KatB, and KatC. The molecular masses, determined by gel filtration chromatography, were estimated to be approximately 270 kDa for KatA, 170 kDa for KatB, and 354 kDa for KatC. These data clearly indicate that KatB is a homodimer whereas KatA and KatC are homotetramers and differ from each other

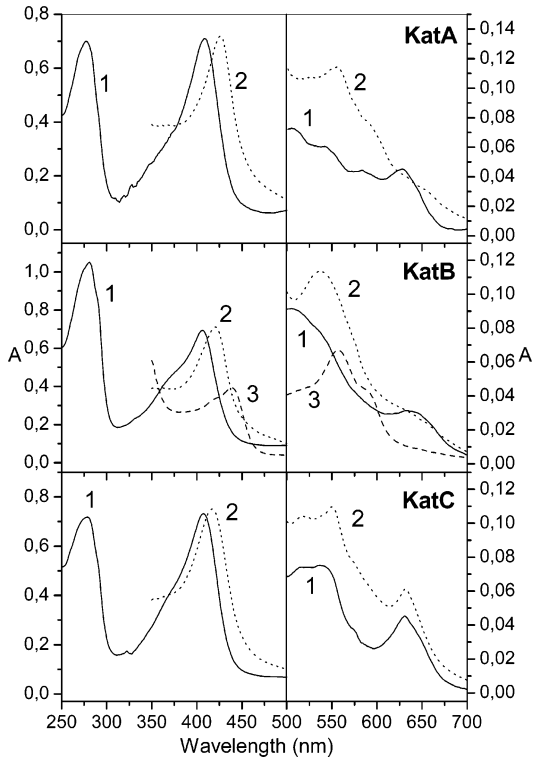

FIGURE 1: Absorption spectra of KatA, KatB, and KatC. Enzymes [(2.5−5.4) × 10^{-6} M] were dissolved in 10 mM potassium phosphate buffer, pH 7.0. Spectra 1: purified proteins. Spectra 2: cyano adducts, obtained by addition of 0.2 M KCN. Spectrum 3: KatB/Fe(II) obtained by addition of 120 mM sodium dithionite under anaerobic conditions.

Table 1: Absorption Maxima and RZ Values for the Three Hydroperoxidases from *S. meliloti*[a]

protein		optical absorbance maxima (nm)					RZ
KatA		409	507 (sh)	543 (sh)	582 (sh)	627	1.01
	+KCN	426		555	588 (sh)	628 (sh)	
KatB		407	504	538 (sh)		636	0.67
	+KCN	421		538	575 (sh)	645 (sh)	
	Fe(II)	438		556	590		
KatC		408	517	549	575 (sh)	630	1.01
	+KCN	417	517	550	575 (sh)	632	

[a] Absorption maxima and RZ (A_{Soret}/A_{280nm}) of the three hydroperoxidases, KatA, KatB, and KatC. The purified proteins [(2.5−5.4) × 10^{-6} M] were dissolved in 10 mM potassium phosphate buffer, pH 7.0. Cyanide complexes were made upon addition of 0.2 M KCN to the ferric proteins. Formation of ferrous proteins [Fe(II)] was obtained by adding 120 mM sodium dithionite under anaerobic conditions.

in containing small and large subunits. The three hydroperoxidases are acidic proteins: the determined isoelectric points are 5.4 (KatA), 5.0 (KatB), and 5.5 (KatC) (data not shown).

The UV−visible spectra of the recombinant proteins are shown in Figure 1, and the absorption maxima and RZ (Reinheitszahl) values are listed in Table 1. KatB shows a spectral pattern typical of catalase-peroxidases: a Soret band at 407 nm and two main broad absorptions at 504 (Q band) and 636 (CT band) nm. KatA and KatC have a Soret band at 409−408 nm and four similar broad absorption maxima in the visible region (two Q and two CT bands) which differ in their relative intensities. The above spectral features indicate an Fe(III)−heme high-spin pentacoordinate coexisting with an Fe(III)−heme high-spin hexacoordinated with water (*32*). Furthermore, as concerning KatA and KatC, the two bands at 543−549 nm and at 627−630 nm are characteristic of heme *b*. In the case of KatC this is uncommon, since large subunit catalases have been shown to contain heme *d* (*3*); typically in heme *d* of HPII catalase from *E. coli* the corresponding bands are shifted to 590 (prominent) and 715 nm (weak) (*33*). Initially, HPII binds heme *b* during assembly, which is subsequently oxidized by the catalase itself during the early rounds of catalysis (*33*). In the case of recombinant *Sinorhizobium* KatC production (expression from a high expression promoter overnight at room temperature) heme conversion could be impaired. However, treatment of KatC with neither various amounts of hydrogen peroxide nor 5 mM ascorbate (the oxidation of which generates low levels of H_2O_2) (*33*) caused spectral shifts indicative of heme *d* formation even at long incubation times (>2 h; data not shown).

The presence of heme *b* in all of the three recombinant proteins was confirmed by the pyridine hemochromogen assay; the spectra of the dithionite-reduced pyridine complexes exhibited the characteristic peaks of iron protoporphyrin IX (heme *b*), with maxima at 418, 525, and 556 nm. On the basis of these spectra, a molar extinction coefficient of 98000 M^{-1} cm^{-1} per heme and a 2.0 heme/dimer ratio were obtained for KatB; moreover, molar extinction coefficient values of 97600 and 78200 M^{-1} cm^{-1} per heme and heme/tetramer ratios equal to 3.0 and 3.4 were calculated for the monofunctional catalases KatA and KatC, respectively. The anaerobic reduction of KatB with sodium dithionite causes a marked shift of the Soret band to 438 nm, together with a significant decrease in intensity (Table 1 and Figure 1, spectrum 3). By contrast, both KatA and KatC were not reduced by sodium dithionite (120 mM).

The UV−visible spectra of the three hydroperoxidase−cyanide complexes (0.2 M cyanide) undergo a characteristic iron(III) high-spin to low-spin conversion (Table 1 and Figure 1, spectrum 2). The KatB−CN^- complex had a Soret band shifted to 421 nm; KatA and KatC exhibit the most and the least pronounced red shift of the Soret band (17 and 9 nm, respectively).

Further characterization of the three enzymes was achieved by means of EPR spectroscopy at low temperature. The EPR spectral patterns of these heme proteins (Figure 2) exhibited two sets of rhombic signals around $g = 6$, with one being clearly dominant, that is in particular occurring for KatC. This behavior could confirm a thermal equilibrium between two Fe(III)−heme high-spin species (penta/hexacoordinated metal ion) that appeared from electronic spectra and which seems evident by freezing. The apparent g tensor values of the predominant signals are reported in Figure 2. The apparent rhombicity (% R) was calculated by the empirical equation % $R = (g_1 - g_2) \times 100/16$, and the values obtained for the three proteins were markedly different: KatA (9.8) > KatC (6.1) > KatB (2.1). This significant decrease in rhombicity from KatA to KatB could correspond to a transition of the ferric catalytic site from one structural motif (a highly rhombic geometry in the case of KatA) to a different one (a nearly axial geometry in the case of KatB).

EPR spectra of the cyanide adducts of the recombinant enzymes have a pattern in the $g = 2$ region representative of low-spin Fe(III)−heme systems, in agreement with the corresponding electronic spectra. The spectrum of KatB−CN^- exhibits resonances at $g = 3.18$, 2.08, and 1.40, whereas

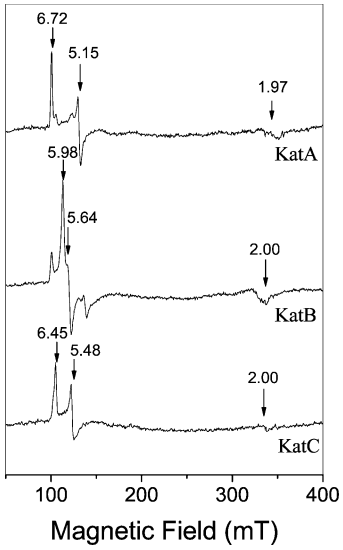

FIGURE 2: Low-temperature EPR spectra of the three recombinant hydroperoxidases. Purified recombinant enzymes (7.2×10^{-6} M KatA; 4.5×10^{-5} M KatB; 4.1×10^{-6} M KatC) were dissolved in 10 mM potassium phosphate, pH 7.0, and 25% glycerol. Conditions were as follows: microwave frequency, 9.456 GHz; microwave power, 10 mW; modulation amplitude, 5 G; modulation frequency, 100 kHz; time constant, 82 ms; temperature, 4 K.

KatA$-CN^-$ and KatC$-CN^-$ show nearly the same pattern, $g = 2.90$, 2.24, and 1.62 for KatA and $g = 2.93$, 2.22, and 1.61 for KatC. The presence of one low-spin pattern suggests that each protein contains only one type of heme cofactor. Further, it is interesting to note that the *g* low-spin component of the KatC$-CN^-$ spectrum differentiates from that of the corresponding HPII$-$cyanide spectrum ($g = 2.34$, 2.23, 1.79) (*34*). From the low-spin components, the crystal field distortion parameters V/λ and Δ/λ were calculated according to Taylor (*35*) together with the V/Δ ratio as well. The axial component Δ/λ (3.96, 4.22, and 4.12 for KatA, KatB, and KatC, respectively) is similar for the three proteins, whereas the rhombic component V/λ of the two monofunctional catalases KatA (2.06) and KatC (2.00) is significantly higher with respect to that obtained for KatB (1.43) and representative of a greater distortion of heme plane. Therefore, for the two monofunctional catalases KatA and KatC the degree of rhombicity V/Δ is comparable (0.52 and 0.48, respectively), whereas it is significantly different for KatB (0.34). This is in good agreement with the apparent rhombicity values (% *R*) calculated from EPR spectra of the recombinant Fe(III) high-spin proteins.

Kinetic Characterization. Specific catalase and peroxidase activities and kinetic parameters of the recombinant proteins are reported in Table 2. A comparison of the specific catalatic activities reveals that KatA is the most active protein (8.54×10^6 units/μmol of heme), while KatB and KatC exhibit lower specific catalase activity (14.0×10^4 and 5.78×10^4 units/μmol of heme, respectively). With a maximum turnover of 279000 s^{-1} for KatA, and turnover rates about 2 orders of magnitude lower for KatB and KatC, *S. meliloti* possesses three catalases displaying very different kinetic properties. The determination of the H_2O_2 concentration at which 50% of maximal activity is attained (apparent K_M, Table 2) reveals a similar broad variation from 1.6 mM (KatB) to 160 mM (KatA). In the case of KatB the apparent K_M was calculated from a double-reciprocal plot, which was revealed to be linear in the 0.5$-$10 mM H_2O_2 concentration range. For the two monofunctional catalases, the double-reciprocal plot is linear between 10 and 200 mM H_2O_2.

Figure 3 shows the pH profiles of catalase activity for the three *S. meliloti* hydroperoxidases. The pH profile of KatB is quite different from that of the monofunctional catalases. The catalatic activity of the latter is essentialy pH-independent between pH 5 and 9, whereas that of KatB shows an optimum around pH 6.5. KatB shows peroxidase activity (optimum pH between 6 and 6.5), with MBTH (227 units/μmol of heme) and ABTS (163 units/μmol of heme) as substrates; conversely, KatA and KatC exhibit no measurable peroxidase activity toward one-electron donors.

Finally, the kinetics of cyanide binding was used to confirm UV$-$visible and EPR data and to probe the heme cavity entrance and proper folding of the three hydroperoxidases (Figure 4). On the basis of the observed spectral changes upon addition of cyanide to ferric KatA, KatB, and KatC (Table 1), the conventional stopped-flow mode was used to follow the spectral transition at the following wavelengths: 425 nm (KatA), 406 nm (KatB), and 427 nm (KatC). The kinetics of cyanide binding to KatA and KatC is monophasic and gives single exponential curves, consistent with a pseudo-first-order kinetics (the original time traces and fits are shown in the insets of Figure 4). The obtained first-order rate constants, k_{obs}, show that with both monofunctional catalases the k_{obs} values linearly increase with the concentration of cyanide (Figure 4). The curve slope yields the apparent second-order rate constant for cyanide binding (k_{on}). The values obtained for KatA and KatC are $(1.2 \pm 0.2) \times 10^6$ M^{-1} s^{-1} and $(5.5 \pm 0.1) \times 10^3$ M^{-1} s^{-1}, respectively, at pH 7 and 30 °C. Since the finite intercepts of 6.9 s^{-1} (KatA) and 46 s^{-1} (KatC) represent k_{off}, from the ratio k_{off}/k_{on} the values for the dissociation constant of the cyanide complex to ferric enzyme and cyanide of 5.8 μM and 8.3 mM for KatA and KatC were calculated. The cyanide binding to the catalase-peroxidase is biphasic, with a fast exponential phase being responsible for more than 90% of absorbance change. Fitting the first rapid phase by a single exponential equation, the bimolecular rate constant for cyanide binding to KatB at pH 7 and 30 °C was determined to be $(2.4 \pm 0.3) \times 10^6$ M^{-1} s^{-1}.

DISCUSSION

Here we have described the overexpression and characterization of the three distinct heme-containing hydroperoxidases from *S. meliloti*. Although other non-heme enzymes, like peroxiredoxins, may contribute to peroxide degradation in this bacterium, these three enzymes are primarily involved in hydrogen peroxide detoxification. Most interestingly, *S. meliloti* expresses a bifunctional catalase-peroxidase (KatB) and two monofunctional catalases, which belong to different clades, namely, to small subunit catalases (KatA) and to large subunit catalases (KatC).

As the amino acid sequence clearly suggests, KatB is a class I hydroperoxidase belonging to the superfamily I of plant, fungal, and bacterial peroxidases and exhibits both a peroxidatic and an overwhelming catalatic activity. The homodimeric (2×85 kDa), heme *b* containing enzyme exhibits spectral characteristics similar to those of other catalase-peroxidases (*10*$-$*12*). Both the absorption maxima

Table 2: Peroxidase and Catalase Specific Activity and Kinetic Parameters[a]

	peroxidase activity (units/μmol of heme)[b]	catalase activity (units/μmol of heme)[c]	K_M (mM)	k_{cat} (s^{-1})[d]	k_{cat}/K_M (s^{-1} M^{-1})
KatA	ND[e]	8.54 ($\pm$0.41) $\times$ 10^6	159 $\pm$ 13	2.79 ($\pm$0.22) $\times$ 10^5	1.75 ($\pm$0.14) $\times$ 10^6
KatB	2.27 ($\pm$0.14) $\times$ 10^2	1.4 ($\pm$0.08) $\times$ 10^5	1.59 $\pm$ 0.07	2.40 ($\pm$0.05) $\times$ 10^3	1.51 ($\pm$0.07) $\times$ 10^6
KatC	ND[e]	5.78 ($\pm$0.14) $\times$ 10^4	150 $\pm$ 20	3.10 ($\pm$0.31) $\times$ 10^3	2.06 ($\pm$0.21) $\times$ 10^4

[a] Means $\pm$ SD; $N = 3$. [b] Peroxidase activity: 1 unit of peroxidase activity catalyzes the oxidation of 1 μmol of MBTH per minute at 25 °C; the assay contained 1 mM hydrogen peroxide, 2 mM DMAB, and 40 μM MBTH in 50 mM phosphate buffer, pH 7.0. [c] Catalase activity: 1 unit of catalase is the amount that catalyzes the formation of 1 μmol of O_2 per minute at 30 °C. The assay contained 5 mM hydrogen peroxide in the case of KatB and 60 mM hydrogen peroxide in the case of KatA and KatC in 67 mM phosphate buffer, pH 7.0. [d] Units of k_{cat} are μmol of O_2 (μmol of heme)$^{-1}$ s^{-1}. [e] ND: not detected.

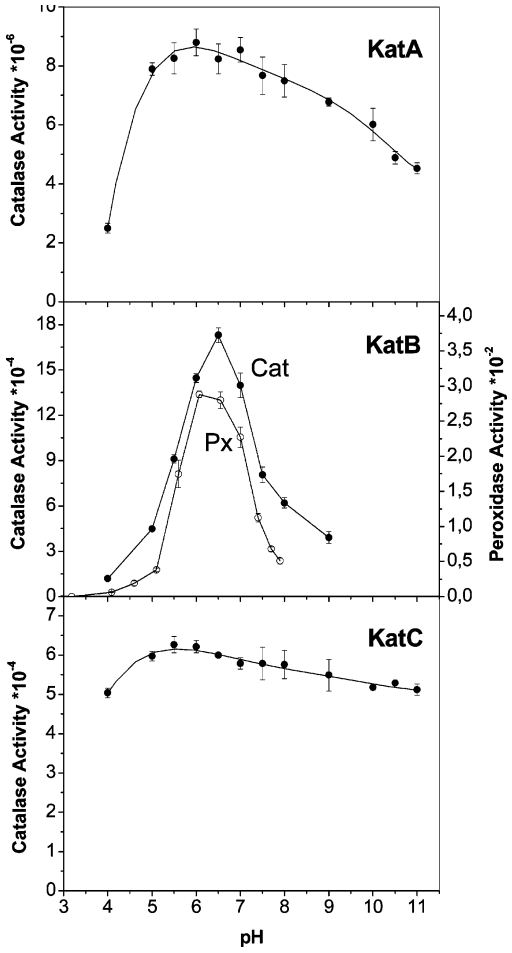

FIGURE 3: pH profile for catalase activity of KatA, KatB, and KatC and for peroxidase activity of KatB. The specific catalase activity (Cat) is μmol of O_2 formed per minute and μmol of heme, determined polarographically at 30 °C, and the specific peroxidase activity (Px) is μmol of MBTH oxidized per minute and μmol of heme, determined spectrophotometrically at 590 nm at 25 °C.

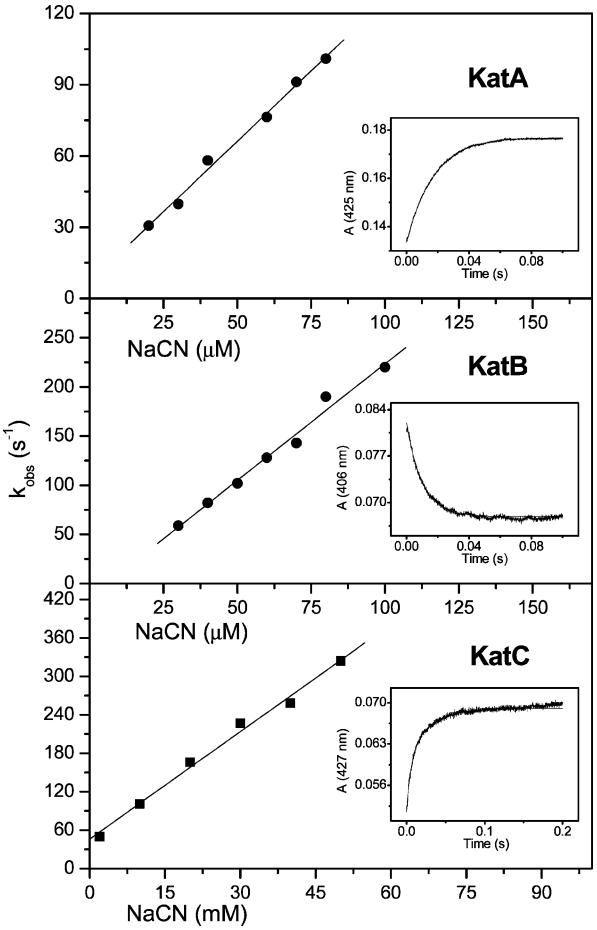

FIGURE 4: Kinetics of cyanide binding to the ferric forms of KatA, KatB, and KatC. Dependence of pseudo-first-order rate constants (k_{obs}) from the cyanide concentration. Representative time traces and fits (single exponential) of the reaction between the ferric proteins (2 μM KatA, 1 μM KatB, and KatC) and 40 μM NaCN (KatA) or 50 μM NaCN (KatB) or 10 mM NaCN (KatC) in 50 mM phosphate buffer, pH 7.0 and 30 °C, are shown in the insets.

in the UV−visible spectrum and the EPR *g* tensor values strongly indicate that *S. meliloti* KatB is a high-spin iron(III) protoporphyrin IX (heme *b*) protein with a histidine (His258, according to the sequence alignment) as the proximal ligand of the metal. In particular, the low-field *g* value (3.18) of the corresponding cyanide adduct fits in the range 3.5−3.0, which is typical of heme proteins with histidine as the proximal ligand and cyanide as the sixth ligand (*36*). These structural assumptions were recently corroborated by the 3D structure of the catalase-peroxidases from *Haloarcula marismortui* (*37*) and *Burkholderia pseudomallei* (*38*). The fact that sodium dithionite reduces only ferric KatB reflects the much more positive reduction potential of the ferric/ferrous couple of catalase-peroxidases in contrast to the monofunctional catalases which have a tyrosinate as the fifth heme ligand. Both the steady-state kinetic parameters and the cyanide binding rate are typical for a bifunctional catalase-peroxidase. KatB is an efficient catalase, with a high affinity for H_2O_2 (K_M 1.59 mM) and a k_{cat}/K_M of 1.5 $\times$ 10^6 s^{-1} M^{-1}. The efficiency of this enzyme fits very well with its housekeeping role already described both in free-living and in symbiotic states (*21*). KatB might therefore function to remove hydrogen peroxide generated during metabolism at low steady-state levels.

In the same way, the homotetrameric structure and the spectral and kinetic characteristics of KatA and KatC are

typical of monofunctional catalases. In particular, spectroscopic features suggest a high-spin Fe(III)−heme *b* catalytic site (*34*, *39*, *40*). According to the sequence alignments, Tyr337 (KatA) and Tyr375 (KatC) are likely to coordinate the heme iron from the proximal side.

Moreover, it is worthy to mention some EPR-related structural peculiarities of the active site of the three hydroperoxidases: (i) the structural modulation of the rhombic distortion as appearing in the EPR spectra of the three recombinant enzymes, (ii) the greater distortion of heme plane for KatA and KatC resulting from the V/λ parameters of the low-spin EPR spectra of the enzyme−cyanide adducts, and (iii) the higher degree of rhombicity V/Δ for the two monofunctional catalases, KatA and KatC.

However, KatA and KatC belong to two different clades according to the phylogenetic classification of monofunctional catalases (*41*): KatA is a small subunit enzyme and member of clade III like the *Proteus mirabilis* catalase and catalases from higher animals, whereas KatC is a large subunit catalase belonging to clade II, as HPII from *E. coli* and the catalase from *Penicillium vitale* (*41*). It must be noted that, in contrast with previous results obtained for other large subunit catalases, which contain a modified heme *b* structure (heme *d*) (*33*), KatC appears to have kept heme *b*. The mechanism of formation of heme *d* from heme *b* seems to be different in *E. coli* and *P. vitale* and is not clearly understood. Interestingly, some variants of *E. coli* HPII (e.g., His392Gln) retained wild-type activity despite having heme *b* (*3*, *42*). In HPII the imidazole ring of His392 is covalently linked to the heme ligand tyrosine (Tyr415) (*42*). In *P. vitale* catalase and *Sinorhizobium* KatC the corresponding residues are a glutamine and a methionine (Met352), respectively. These findings show that heme *d* is not necessarily required for catalytic activity in the large subunit enzymes and that the mechanisms leading to heme *d* may be different in these enzymes (*3*). In the case of *S. meliloti* KatC, several findings underline the existence of only one heme type, namely, heme *b*: (i) the absorption maxima of the recombinant protein and of the dithionite-reduced pyridine complex of the heme extracted from KatC, (ii) the presence of only one heme species seen in EPR spectroscopy, and, finally, (iii) the monophasic kinetics of cyanide binding observed in the conventional stopped-flow experiments. But it has to be noted that the investigated protein was expressed heterologously, which could cause some problems with proper folding and heme conversion and may explain the low affinity for cyanide ($K_D = 8.3$ mM). It would be worth comparing the recombinant protein with the native protein purified from *S. meliloti*.

Nevertheless, as in the case of KatB, the kinetic parameters of the two monofunctional catalases are in good agreement with the data already obtained about their physiological roles (*19*, *21*, *22*). KatA exhibits the highest specific activity and the lowest affinity for the substrate. This again fits well with its physiological characteristics. Indeed, KatA is the sole H_2O_2-inducible catalase of *S. meliloti* (*21*). Thus, the expression of the *katA* gene is largely enhanced when the cells are facing an oxidative stress situation. This seems to be particularly the case with symbiotic bacteroids, where the high rate of bacteroid respiration and the stringent conditions required to reduce nitrogen may induce an oxidative stress situation (*22*). In this framework, the K_M is not the determinant parameter; furthermore, it should be noted that a value up to 1.1 M has been reported for the apparent K_M of beef liver catalase (*43*). On the other hand, *katC* gene expression is also induced by stress situations (heat, salt, or ethanol stress) (*21*). This is in agreement with the fact that some large subunit catalases are more resistant to denaturation by heat, salt, ethanol, and chemical denaturants and that their expression is often induced by stressful conditions or at the end of exponential growth (*44*).

Unlike bacteria such as *E. coli*, *P. mirabilis*, or *Synechocystis* PCC 6803, *S. meliloti*, as other Rhizobia (e.g., *Bradyrhizobium japonicum*, *Sinorhizobium fredii*, *Rhizobium leguminosarum* bv. *trifolii*, and *R. leguminosarum* bv. *phaseoli*), contains three catalases (*21*). In this framework, it is interesting to note that bacteria which interact with other organisms, such as *Klebsiella pneumoniae*, also contain three catalases (*45*). Sophisticated regulation of the three HP of *S. meliloti* occurs not only in batch cultures but also during the symbiotic interaction (*22*). Thus, *S. meliloti* has kept a panel of enzymes which enables it to adapt to various environmental conditions both in the soil as a free-living organism and in root nodules as a symbiont. The combination of the regulatory processes (e.g., *katA* induced by H_2O_2) and of the kinetic parameters of the three hydroperoxidases appears to lead to an optimization of the *S. meliloti* capacity of H_2O_2 scavenging.

REFERENCES

1. Halliwell, B. (1996) Free radicals, proteins and DNA: oxidative damage versus regulation, *Biochem. Soc. Trans. 24*, 1023−1027.
2. Fridovich, I. (1986) Biological effects of the superoxide radical, *Arch. Biochem. Biophys. 247*, 1−11.
3. Nicholls, P., Fita, I., and Loewen, P. C. (2001) Enzymology and structure of catalases, *Adv. Inorg. Biochem. 51*, 51−106.
4. Welinder, K. G., Mauro, J. M., and Norskov-Lauritsen, L. (1992) Structure of plant and fungal peroxidases, *Biochem. Soc. Trans. 20*, 337−340.
5. Ferrari, R. P., and Traversa, S. (2000) Structure function relationships amongst members of animal peroxidase family of proteins, in *The peroxidase multigene family of enzymes*, pp 114−120, Springer-Verlag, Heidelberg.
6. Nadler, V., Goldberg, I., and Hochman, A. (1986) Comparative study of bacterial catalases, *Biochim. Biophys. Acta 882*, 234−241.
7. Switala, J., and Loewen, P. C. (2002) Diversity of properties among catalases, *Arch. Biochem. Biophys. 401*, 145−154.
8. Welinder, K. G. (1991) Bacterial catalase-peroxidases are gene duplicated members of the plant peroxidase superfamily, *Biochim. Biophys. Acta 1080*, 215−220.
9. Cendrin, F., Jouve, H. M., Gaillard, J., Thibault, P., and Zaccai, G. (1994) Purification and properties of a halophilic catalase-peroxidase from *Haloarcula marismortui*, *Biochim. Biophys. Acta 1209*, 1−9.
10. Johnson, C. H., Klotz, M. G., York, J. L., Kruft, V., and McEwen, J. E. (2002) Redundancy, phylogeny and differential expression of *Histoplasma capsulatum* catalases, *Microbiology 148*, 1129−1142.
11. Clairborne, A., and Fridovich, I. (1979) Purification of the o-dianisidine peroxidase from *Escherichia coli*, *J. Biol. Chem. 254*, 4245−4252.
12. Hochman, A., and Goldberg, I. (1991) Purification and characterization of a catalase-peroxidase and a typical catalase from the bacterium *Klebsiella pneumoniae*, *Biochim. Biophys. Acta 1077*, 299−307.
13. Jakopitsch, C., Ruker, F., Regelsberger, G., Dockal, M., Peschek, G. A., and Obinger, C. (1999) Catalase-peroxidase from the cyanobacterium *Synechocystis* PCC 6803: cloning, overexpression in *Escherichia coli*, and kinetic characterization, *Biol. Chem. 380*, 1087−1096.

14. Mulvey, M. R., Switala, J., Borys, A., and Loewen, P. C. (1990) Regulation of transcription of *katE* and *katF* in *Escherichia coli*, *J. Bacteriol. 172*, 6713−6720.
15. Loewen, P. C., Switala, J., and Triggs-Raine, B. L. (1985) Catalases HPI and HPII in *Escherichia coli* are induced independently, *Arch. Biochem. Biophys. 243*, 144−149.
16. Barnett, M. J., Fisher, R. F., Jones, T., Komp, C., Abola, A. P., Barloy-Hubler, F., Bowser, L., Capela, D., Galibert, F., Gouzy, J., Gurjal, M., Hong, A., Huizar, L., Hyman, R. W., Kahn, D., Kahn, M. L., Kalman, S., Keating, D. H., Palm, C., Peck, M. C., Surzicky, R., Wells, D. H., Yeh, K., Davis, R. W., Federspiel, N. A., and Long, S. R. (2001) Nucleotide sequence and predicted functions of the entire *Sinorhizobium meliloti* pSymA megaplasmid, *Proc. Natl Acad. Sci. U.S.A. 98*, 9883−9888.
17. Finan, T. M., Weidner, S., Wong, K., Buhrmester, J., Chain, P., Vorholter, F. J., Hernandez-Lucas, I., Becker, A., Cowie, A., Gouzy, J., Golding, B., and Puhler, A. (2001) The complete sequence of the 1,683-kb pSymB megaplasmid from the N_2-fixing endosymbiont *Sinorhizobium meliloti*, *Proc. Natl. Acad. Sci. U.S.A. 98*, 9889−9894.
18. Capela, D., Barloy-Hubler, F., Gouzy, J., Bothe, G., Ampe, F., Batut, J., Boistard, P., Becker, A., Boutry, M., Cadieu, E., Dréano, S., Gloux, S., Godrie, T., Goffeau, A., Kahn, D., Kiss, E., Lelaure, V., Masuy, D., Pohl, T., Portetelle, D., Puhler, A., Purnelle, B., Ramsperger, U., Renard, C., Thébault, P., Vandenbol, M., Weidner, S., and Galibert, F. (2001) Analysis of the chromosome sequence of the legume symbiont *Sinorhizobium meliloti* strain 1021, *Proc. Natl. Acad. Sci. U.S.A. 98*, 9877−9882.
19. Hérouart, D., Sigaud, S., Moreau, S., Frendo, P., Touati, D., and Puppo, A. (1996) Cloning and characterization of the katA gene of *Rhizobium meliloti* encoding a hydrogen peroxide-inducible catalase, *J. Bacteriol. 178*, 6802−6809.
20. Long, S. R. (1989) *Rhizobium*-legume nodulation: life together in the underground, *Cell 56*, 203−214.
21. Sigaud, S., Becquet, V., Frendo, P., Puppo, A., and Hérouart, D. (1999) Differential regulation of two divergent *Sinorhizobium meliloti* genes for HPII-like catalases during free-living growth and protective role of both catalases during symbiosis, *J. Bacteriol. 181*, 2634−2639.
22. Jamet, A., Sigaud, S., Van de Sype, G., Puppo, A., and Hérouart, D. (2003) Expression of the bacterial catalase genes during *Sinorhizobium meliloti-Medicago sativa* symbiosis and their crucial role during the infection process, *Mol. Plant Microbe Interact. 16*, 217−225.
23. Ausubel, F. M., Brent, R., Kingston, R. E., Moore, D. D., Seidman, J. G., Smith, J. A., and Struhl, K. (1993) *Current protocols in molecular biology*, Green Publishing Associates, New York.
24. Bradford, M. M. (1993) A rapid and sensitive method for the quantitation of microgram quantities of protein utilizing the principle of protein-dye binding, *Anal. Biochem. 72*, 248−254.
25. Laemmli, U. K. (1970) Cleavage of structural proteins during the assembly of the head of bacterio phage T4, *Nature 227*, 680−685.
26. Clare, D. A., Duong, M. N., Darr, D., Archibald, F., and Fridovich, I. (1984) Effects of molecular oxygen on detection of superoxide radical with nitroblue tetrazolium and on activity stains for catalase, *Anal. Biochem. 140*, 532−537.
27. Furhop, J. H., and Smith, K. M. (1975) Hemes-Determination as pyridine hemochromes, in *Laboratory Methods in Porphyrin and Metalloporphyrin Research*, pp 48−51, Elsevier, Amsterdam.
28. Rørth, M., and Jensen, P. K. (1967) Determination of catalase activity by means of the Clark electrode, *Biochim. Biophys. Acta 139*, 171−173.
29. Ngo, T. T., and Lenhoff, H. M. (1980) A sensitive and versatile chromogenic assay for peroxidase and peroxidase coupled reactions, *Anal. Biochem. 105*, 389−397.
30. Childs, R. E., and Bardsley, W. G. (1975) The steady-state kinetics of peroxidase with 2,2′-azino-di-(3-ethylbenzthiazoline-6-sulphonic acid) as chromogen, *Biochem. J. 145*, 93−103.
31. Kerschbaumer, R. J., Hirschl, S., Kaufmann, A., Ibl, M., Koenig, R., and Himmler, G. (1997) Single-chain Fv fusion proteins suitable as coating and detecting reagents in a double antibody sandwich enzyme-linked immunosorbent assay, *Anal. Biochem. 249*, 219−227.
32. Heering, H. A., Indiani, C., Regelsberg, G., Jakopitsch, C., Obinger, C., and Smulevich, G. (2002) New insights into the heme cavity structure of catalase-peroxidase: a spectroscopic approach to the recombinant *Synechocystis* enzyme and selected distal cavity mutants, *Biochemistry 41*, 9237−9247.
33. Loewen, P. C., Switala, J., von Ossowski, I., Hillar, A., Christie, A., and Tattrie, B. (1993) Catalase HPII of *Escherichia coli* catalyzes the conversion of protoheme to cis-heme d, *Biochemistry 32*, 10159−10164.
34. Peng, Q., Timkovich, R., Loewen, P. C., and Peterson, J. (1992) Identification of heme macrocycle type by near-infrared magnetic circular dichroism spectroscopy at cryogenic temperatures, *FEBS Lett. 309*, 157−160.
35. Taylor, C. P. S. (1977) The EPR low spin heme complexes, *Biochim. Biophys. Acta 491*, 137−149.
36. Ferrari, R. P., Laurenti, E., Cecchini, P. I., Gambino, O., and Sondergaard, I. (1995) Spectroscopic investigations on the highly purified lactoperoxidase Fe(III)-heme catalytic site, *J. Inorg. Biochem. 58*, 109−127.
37. Yamada, Y., Fujiwara, T., Sato, T., Igarashi, N., and Tanaka, N. (2002) The 2.0 Å crystal structure of catalase-peroxidase from *Haloarcula marismortui*, *Nat. Struct. Biol. 9*, 691−695.
38. Carpena, X., Loprasert, S., Mongkolsuk, S., Switala, J., Loewen, P. C., and Fita, I. (2003) Catalase-peroxidase KatG of *Burkholderia pseudomallei* at 1.7 Å resolution, *J. Mol. Biol. 327*, 475−489.
39. Ivancich, A., Jouve, H. M., Sartor, B., and Gaillard, J. (1997) EPR investigation of Compound I in *Proteus mirabilis* and Bovin liver catalases: formation of porphyrin and tyrosyl radical intermediates, *Biochemistry 36*, 9356−9364.
40. Torii, K., Iizuka, T., and Ogura, Y. (1970) Magnetic susceptibility and EPR measurements of catalase and its derivatives, *J. Biochem. 68*, 837−841.
41. Klotz, M. G., and Loewen, P. C. (2003) The molecular evolution of catalatic hydroperoxidases: evidence for multiple lateral transfer of genes between prokaryota and from bacteria into eukaryota, *Mol. Biol. Evol. 20*, 1098−1112.
42. Maté, M., Sevinc, M. S., Hu, B., Bujonst, J., Bravo, J., Switala, J., Ens, W., Loewen, P. C., and Fita, I. (1999) Mutants that alter the covalent structure of catalase hydroperoxidase II from *Escherichia coli*, *J. Biol. Chem. 274*, 27717−27725.
43. Maté, M., Murshudov, G., Bravo, J., Melik-Adamyan, W., Loewen, P. C., and Fita, I. (2001) Heme-catalases, in *Handbook of metalloproteins*, Vol. 1, pp 486−502, J. Wiley & Sons, Chichester, U.K.
44. Switala, J., O'Neil, J. O., and Loewen, P. C. (1999) Catalase HPII from *Escherichia coli* exhibits resistance to denaturation, *Biochemistry 38*, 3895−3901.
45. Goldberg, I., and Hochman, A. (1989) Three different types of catalases in *Klebsiella pneumoniae*, *Arch. Biochem. Biophys. 268*, 124−128.

BI048836S